Time Scales of Climate Response

RONALD J. STOUFFER

NOAA/Geophysical Fluid Dynamics Laboratory, Princeton, New Jersey

(Manuscript received 9 April 2003, in final form 16 July 2003)

ABSTRACT

A coupled atmosphere–ocean general circulation model (AOGCM) is integrated to a near-equilibrium state with the normal, half-normal, and twice-normal amounts of carbon dioxide in the atmosphere. Most of the ocean below the surface layers achieves 70% of the total response almost twice as fast when the changes in radiative forcing are cooling as compared to the case when they are warming the climate system. In the cooling case, the time to achieve 70% of the equilibrium response in the midoceanic depths is about 500–1000 yr. In the warming case, this response time is 1300–1700 yr. In the Pacific Ocean and the bottom half of the Atlantic Ocean basins, the response is similar to the global response in that the cooling case results in a shorter response time scale. In the upper half of the Atlantic basin, the cooling response time scales are somewhat longer than in the warming case due to changes in the oceanic thermohaline circulation. In the oceanic surface mixed layer and atmosphere, the response time scale is closely coupled. In the Southern Hemisphere, the near-surface response time is slightly faster in the cooling case. However in the Northern Hemisphere, the near-surface response times are faster in the warming case by more than 500 yr at times during the integrations. In the Northern Hemisphere, both the cooling and warming cases have much shorter response time scales than found in the Southern Hemisphere. Oceanic mixing of heat is the key in determining these time scales. It is shown that the model's simulation of present-day radiocarbon and chlorofluorocarbon (CFC) distributions compares favorably to the observations indicating that the quantitative time scales may be realistic.

1. Introduction

When the radiative forcing of the planet changes, various components of the coupled ocean–atmosphere–land surface system respond to those changes with differing time scales. In the physical climate system, the atmosphere–ocean–land surface–sea ice system, typically the shortest response times are found in the atmosphere. The atmosphere can come into equilibrium with new lower boundary conditions on time scales from days to weeks. The longest response time scales to a change in radiative forcing in the physical climate system are found in the deep ocean. These response time scales can be longer than 1000 yr.

One question that arises is: How long are the response time scales? A second question is: Does the response time scale depend on the sign of the change in radiative forcing? A change in the radiative forcing that heats the ocean surface makes the ocean more stable, isolating the deeper waters from the surface. A change of the radiative forcing, which tends to cool the ocean surface, makes the ocean more unstable. This promotes mixing between the surface and deeper waters. Therefore, it is expected that the response time scale of the physical climate system to these two different perturbations may be very different.

Earlier Manabe et al. (1991) investigated these questions using model integrations of 100 yr in length, looking at the transient response of the model to heating and cooling perturbations. They found that the heat anomalies penetrate to a much greater depth in the integration when the ocean surface is cooled, as compared to the case when it is warmed in agreement with the discussion above. The results presented here show that those findings also apply over much longer time scales. Here, these questions are investigated using a coupled atmosphere–ocean general circulation model (AOGCM), which is time integrated to a near-equilibrium state.

The question of climate response time scale is important in understanding past climate changes. If the response time scales are long, the climate will continue to evolve long after the radiative forcing is changed or stabilized. This fact complicates the interpretation of the paleoclimate record. It can be hard to relate an inferred change in climate to the change in forcing. This question of time scale of response is also important for future climate changes in that the climate will continue to evolve after the greenhouse gas concentration are stabilized (Stouffer and Manabe 1999; Cubasch et al. 2001).

Corresponding author address: R. J. Stouffer, NOAA/Geophysical Fluid Dynamics Laboratory, Princeton, NJ 08542.
E-mail: Ronald.Stouffer@noaa.gov

Recently, Stouffer and Manabe (1999) published results from an AOGCM integrated to equilibrium where the CO_2 concentration was twice its normal value. Another integration of the same AOGCM has reached equilibrium where the CO_2 concentration is half its normal value (Stouffer and Manabe 2003). The response time scale can be computed using the cooling and warming integrations. By comparing the time it takes to reach a given fraction of the total equilibrium response in these integrations, the questions of the response time scale and how the response time scale depends on the sign of the change in radiative forcing is investigated.

In the following section, the model and experimental design are described. The third section makes an assessment of the mixing in the oceanic component of the AOGCM by comparing the radiocarbon simulation in the control integration to observations. In the last two sections, the results of the experiment are presented and discussed.

2. Model description and experimental design

The coupled model is only briefly described here. For more details see Manabe et al. (1991) and the references therein. In the 2001 Intergovernmental Panel on Climate Change (IPCC) Working Group I report, the label for this model is GFDL_R15_a (see Table 9.1 in Cubasch et al. 2001). The AOGCM has a global domain with realistic geography. The atmospheric component has nine unevenly spaced vertical levels. The horizontal distributions of the predicted variables are represented by spherical harmonics and associated gridpoint values with 4.5° latitude by 7.5° longitude spacing (Gordon and Stern 1982). Sunshine varies seasonally, but not diurnally. Cloud cover is predicted based on relative humidity. A simple land surface model computes the fluxes of heat and water (Manabe 1969). The oceanic component of the coupled model employs a finite-difference technique using a grid spacing of 4.5° latitude by 3.75° longitude. There are 12 unevenly spaced levels in the ocean. Subgrid-scale, oceanic tracer mixing occurs on density surfaces (Redi 1982; Tziperman and Bryan 1993). The sea ice model computes ice thickness based on thermodynamic heat balance and movement of the ice by ocean currents. The atmospheric, ocean, and sea ice components exchange fluxes of heat, water, and momentum once per day. To prevent large climate drifts, the fluxes of heat and water are adjusted using values that vary seasonally, but not on longer time scales. For this experiment, it is important that the control climate be as realistic as possible since the climate sensitivity is a function of the control climate state (Spelman and Manabe 1984).

The relative simplicity of the subgrid-scale parameterizations and the fact that diurnal variation is not included, allows the AOGCM to be time integrated to a statistical equilibrium on present-day computers. Three 5000-yr integrations are used in this study. In the first ($2 \times CO_2$), CO_2 increases at a rate of 1% yr^{-1} (compounded) to doubling (year 70). The CO_2 concentration is then held fixed at twice its normal value for the remainder of the integration. In the second integration ($\frac{1}{2} \times CO_2$), CO_2 decreases at a rate of 1% yr^{-1} to the point where it is half its initial value (year 70) when the CO_2 concentration is held fixed. The third integration is the control when the CO_2 concentration is held constant throughout the integration.

In a preliminary $\frac{1}{2} \times CO_2$ integration, the sea ice thickness became very thick, more than 100 m. In areas of large negative heat flux adjustment, places where heat is being removed from the ocean, the ocean is isolated from the atmosphere by the uncontrolled growth of sea ice and by the fact that the sea ice parameterization does not allow for leads in the ice. The various oceanic damping mechanisms (advection, convection, etc.) are not large enough to balance the negative heat flux adjustment term and the sea ice continues to grow. In order to control growth of the sea ice thickness, the sea ice thickness is limited to 10 m. During the $\frac{1}{2} \times CO_2$ integration presented here, whenever the sea ice thickness exceeds this critical value, the thickness is set to 10 m. The difference between the original thickness and 10 m is converted into an equivalent amount of heat and water flux. The water flux is allowed to impact the surface salinities in the ocean. The heat flux, on the other hand, enters into the surface heat budget at the ice–atmosphere interface, allowing the atmosphere to ventilate heat. This technique controls growth of the sea ice (extent and thickness). In the other two integrations the sea ice thickness never reaches 10 m. Therefore this technique is not needed and has no impact in those integrations.

By the end of the two perturbation integrations, the climate is nearly in equilibrium with the forcing. The equilibrium conditions from each integration are computed by taking a century time average for the years 4901–5000. Here the atmospheric and oceanic temperature response time scales are used as a surrogate for the response time scale of the physical coupled system. The transient response is computed using century time averages taken from various time intervals in the perturbation integrations and comparing that climate to the century time average from the control (years 4901–5000). By comparing the time required to reach 30% and 70% of the total response, the effect of the sign of the change in radiative forcing on the rate of the climate response is investigated.

As will be seen in the figures, two issues need to be noted when using this method of analysis. One issue is that the ratio (transient response divided by the equilibrium response) is unreliable when the equilibrium response is very small (near zero). For example, the response time scales near 1-km depth at 75°N in the $\frac{1}{2} \times CO_2$ integration suffer from this problem. A second issue is that the water temperature cannot fall below the freezing point due to sea ice formation. Since annually averaged temperatures are used to compute the ratios,

this can lead to distorted estimates of the response time scales.

3. Evaluation of ocean mixing

Before investigating the climate response times obtained from this model, it is important to assess how realistic the mixing is represented in the model. Dixon et al. (1996) made an assessment of the oceanic mixing in this model using chlorofluorocarbons (CFCs). These oceanic tracers, which are useful for evaluating mixing processes on time scales shorter than 100 years, are simulated quite well by the model. As noted by Dixon et al. (1996), it is possible that the good CFC simulation results from offsetting model errors. The model simulation of the circumpolar winds is too weak when compared to the observations, which would tend to reduce the vertical mixing of tracers. The use of the Redi isopyncal mixing scheme tends to result in too much mixing of oceanic tracers (England 1995; Robitaille and Weaver 1995). The opposing tendencies tend to cancel, yielding the good simulation of CFCs, indicating that the magnitude of the model's oceanic mixing of the present-day climate is realistic. However, it is impossible to estimate to what extent this error cancellation occurs in the perturbed climates.

On longer time scales, tracers other than CFCs must be used. Here, radiocarbon, $\Delta^{14}C$, obtained from the Western Pacific Geochemical Ocean Sections Study (GEOSECS) track is used to assess model mixing on centennial to millennial time scales (for more examples using radiocarbon as an oceanic tracer, see Toggweiler et al. 1989; Toggweiler and Samuels 1993; England and Rahmstorf 1999). Using the method described in Toggweiler et al. (1989), a radiocarbon tracer is included in the control integration of the AOGCM. Two differing assumptions are used for the influence of sea ice on the fluxes of $\Delta^{14}C$ in the model. In one, the air–sea flux of $\Delta^{14}C$ is set to zero whenever sea ice is present at the grid location. The second assumption is more complex. For sea ice thickness greater than 3 m, the surface flux is zero. For thickness between 0 and 3 m, the flux is linearly interpolated between its full value and zero using the sea ice thickness. Results using both assumptions are shown. These two assumptions should bracket the influence of sea ice on the $\Delta^{14}C$ distribution in the world oceans.

Fallout from the nuclear bomb tests has greatly influenced the $\Delta^{14}C$ distribution in the upper ocean (above 1-km depth) in the observations. The comparison of model to observations will be constrained to deeper layers of the ocean. The model simulations using both assumptions for the tracer flux through sea ice show a maximum $\Delta^{14}C$ depletion of about 200–220 parts per thousand (ppt) around 3 km in the North Pacific Ocean (Figs. 1a,b). This is slightly smaller than the observed value of 240 ppt (Fig. 1c). Near Antarctica at 1-km depth, the model $\Delta^{14}C$ values are near 120–130 ppt

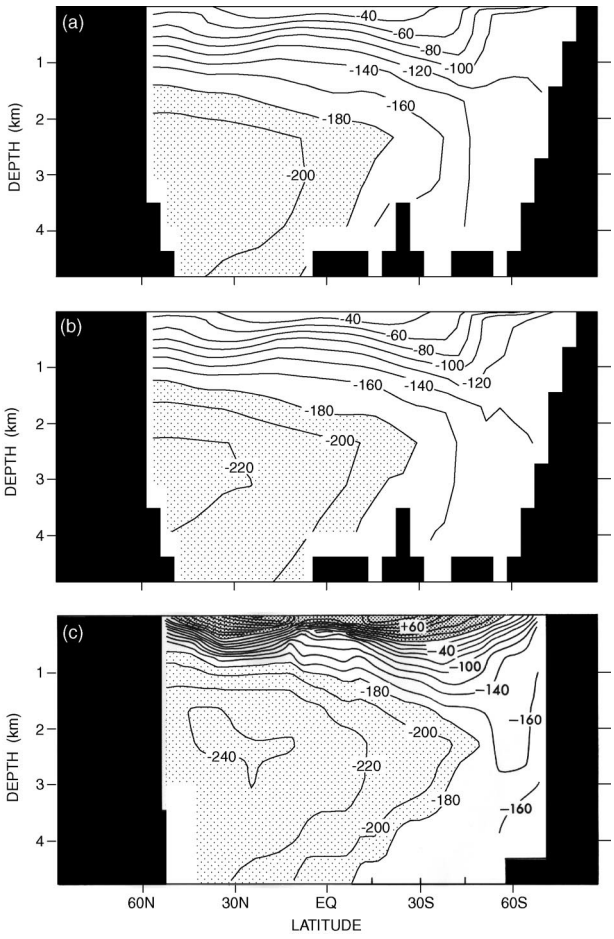

FIG. 1. Latitude vs depth section of $\Delta^{14}C$ (ppt) along the western Pacific GEOSECS track. (a) Model assuming no carbon flux through sea ice, independent of ice thickness. (b) Model assuming sea ice has the following effect on carbon fluxes: For sea ice thickness >3 m, the carbon flux is zero. For sea ice thickness between 3 and 0 m, the carbon flux is linearly interpolated between zero and the full carbon flux using the sea ice thickness. (c) Observations [data source Ostlund et al. (1987), figure from Toggweiler and Samuels (1993)].

(Figs. 1a,b). Again, this is slightly smaller than the observed value of about 150 ppt (Fig. 1c). Toggweiler and Samuels (1993) argue that the difference in the $\Delta^{14}C$ depletion between Antarctica surface waters and the deep North Pacific is strongly related to the long-time-scale mixing in the model. In their study, they find that most models have too large a difference, indicating too much mixing. Here, both model and observed differences are just over 100 ppt, indicating that the mixing found in this model is fairly realistic on the long time scales. This result gives creditability to the quantitative response time scales that follow.

4. Response time scales

In this section, the time required to reach 30% and 70% of the total response is discussed. Results from the

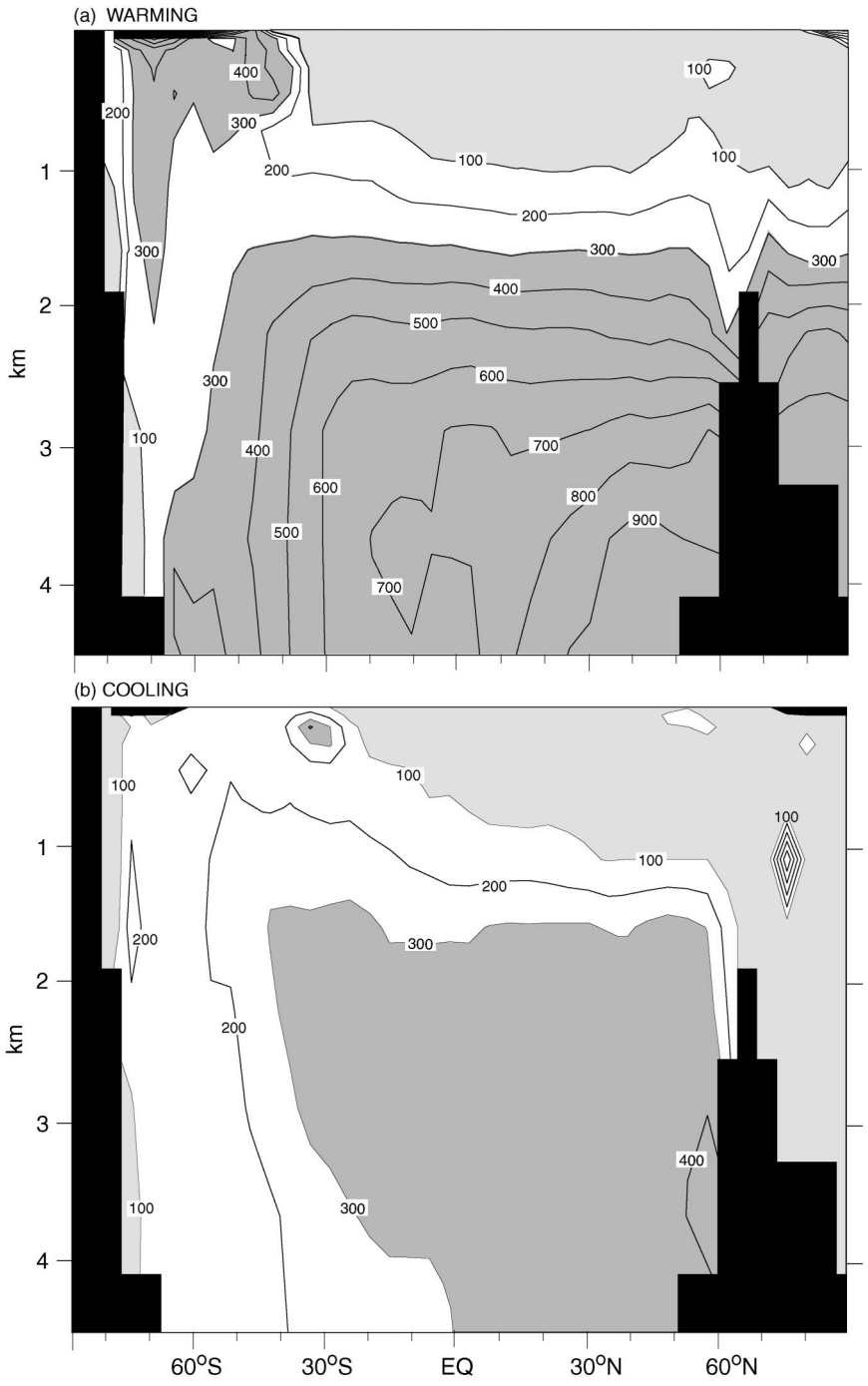

FIG. 2. The time (years) to reach 30% of the total, equilibrium response from the beginning of the integration (the first occurrence). The fraction of the total response is computed by dividing the response at any given time by the total response at each grid location: (a) the zonal mean latitude vs depth section of the local response time scales obtained using data from the $2 \times CO_2$ integration, and (b) the $\frac{1}{2} \times CO_2$ integration.

global ocean are shown for the 30% case, while the global ocean and both major basins are shown for the 70% case. The response of the hemispheric surface air temperature is shown near the end of this section.

The response time scale is generally smaller near the ocean's surface and increases with depth (Fig. 2). This is not the case in the Circumpolar Ocean where the surface waters mix to great depth so that the response times are long and tend to be fairly constant with depth. The time required to reach 30% of the total response in

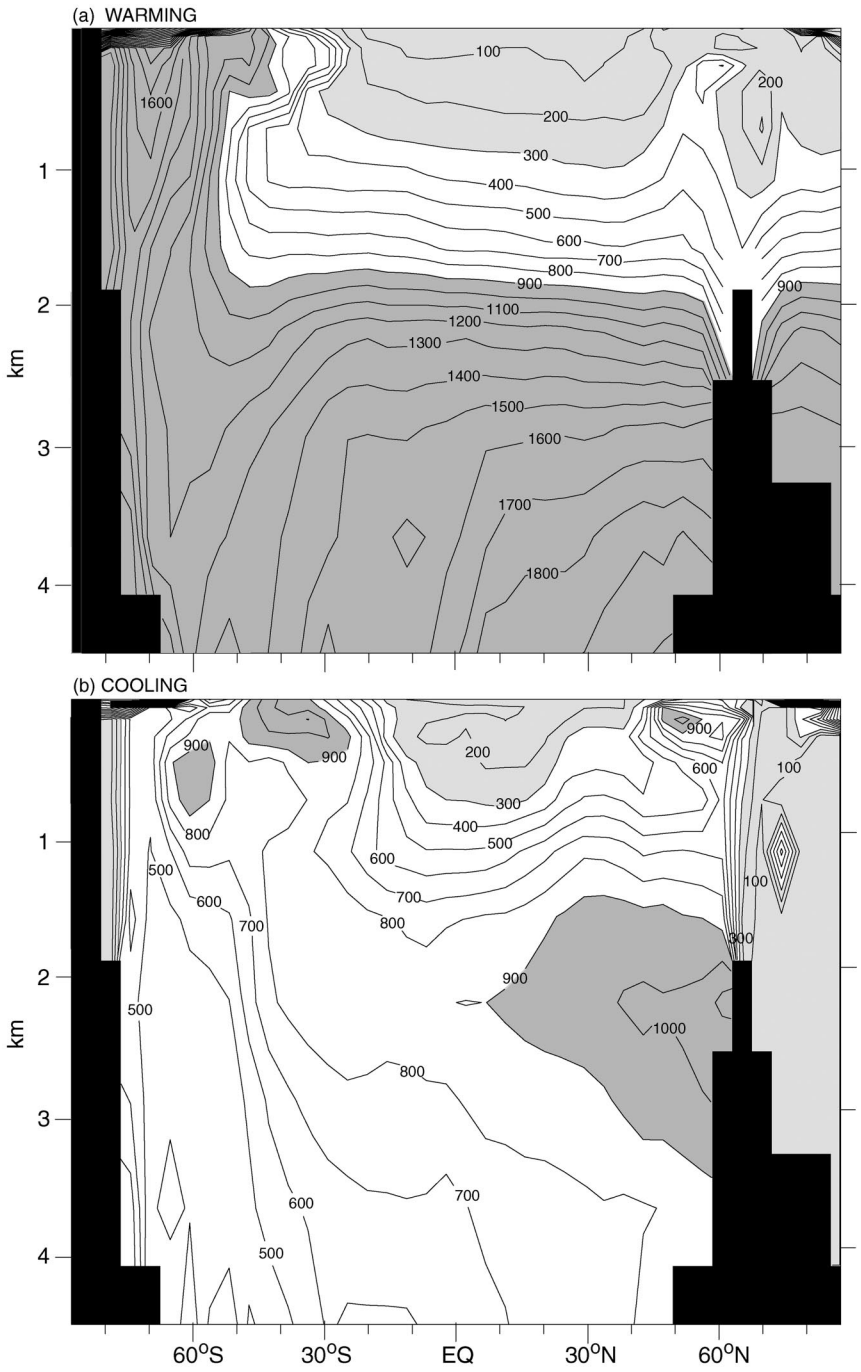

FIG. 3. As in Fig. 2 but for 70% of the response.

the warming case (Fig. 2a) varies from less than 100 yr above 750 m, northward of 30°S, to more than 900 yr found near the ocean bottom at 45°N. In the Circumpolar Ocean, the response time scale is about 300 yr throughout the depth of the ocean. In the cooling case (Fig. 2b), the response time scale for 30% of the total response is about 300 yr throughout most of the world ocean below 2 km. It is also less than 100 yr near the ocean surface (about 500 m) and throughout the ocean depth around Antarctica.

The time required to reach 70% of the total response is naturally larger than discussed above. In the warming case (Fig. 3a), the longest response time scales are again located near the bottom of the ocean, near 50°N. In this location, it takes about 2000 yr to reach 70% of the total equilibrium response. In the cooling case (Fig. 3b),

one notes that the longest response times are located at 2.2-km depth near 50°N. In this case, it takes about 1000 yr to reach 70% of the equilibrium response. From the geographical maps of the response time scales computed at the various oceanic levels (not shown), it is found that the longest response time scales at depth occur along oceanic ridges, places of increased vertical mixing of the deep waters.

By comparing the response time scales for the ocean waters obtained from the increased and decreased CO_2 integrations (Figs. 2a,b or 3a,b), it is noted that the response time scales are much shorter for the cooling case than for the warming case throughout much of the World Ocean. As noted in the introduction, the ocean surface is being heated in the warming case, thus making the ocean more stable, inhibiting the penetration of heat into the ocean. In the warming case, the deeper waters are becoming more isolated from the surface waters and oceanic convection and other vertical mixing processes become less frequent and less intense (Manabe et al. 1991). This inhibits the penetration of heat into the ocean, causing the relatively long response time scales away from the ocean surface. In the cooling case, the ocean surface is being cooled, destabilizing the ocean. As the ocean surface becomes denser, it leads to more intense vertical mixing and convection. This additional mixing allows the heat anomaly at the surface to penetrate into the interior of the ocean at a faster rate than in the control or warming integrations. This lead to relatively longer response times near the ocean surface and relatively shorter response time scales in the ocean interior to changes in the radiative forcing, which tend to cool the surface.

Manabe et al. (1991) noted this effect earlier in transient AOGCM integrations as noted in the introduction. They found that the heat anomalies penetrated to a much greater depth in the integration when the ocean surface is cooled as compared to the case where it is warmed. In these 100-yr integrations, the atmospheric CO_2 concentration increased or decreased at a rate of 1% yr^{-1}. The results presented here show that those findings also apply over much longer time scales. These changes are discussed further below.

Looking at the sections obtained from the ocean basins, one can see the effect of changes in the ocean circulation. The conclusions one would reach by inspecting the Pacific figures are very similar to the conclusion obtained by inspecting the global figures (cf. Figs 4a,c to Figs. 3a,b). The situation is different in the Atlantic basin (Figs. 4b,d). There, the time taken to achieve 70% of the total response is longer in the cooling integration than in the warming in the waters above 2 km. In the bottom half of the basin, the results are similar to the global picture discussed above in that the warming response time scales are much longer than the cooling response time scales.

The shorter response time scale in the upper part of the Atlantic basin (above 2 km or so) in the warming case results from the changes in the thermohaline circulation (THC) and associated high-latitude oceanic convection. This is most easily seen by comparing Pacific and Atlantic response time scales (Figs. 4a,b). Near the beginning of the integration of the warming case, the THC slows down as the climate warms. The weakening of the THC in this model is mainly due to the increased freshwater flux at the ocean surface in high latitudes, although the changes in heat flux also play a role in the weakening (Dixon et al. 1999). The slowing of the THC decreases the northward heat transport in the model's Atlantic Ocean (Manabe et al. 1991). This allows the waters above 2 km in the Tropics and subtropics to warm more rapidly than would otherwise be expected, leading to the shorter time scales of response in the Atlantic compared to the Pacific Ocean. In higher latitudes, the reduction of the vertical mixing, resulting from the weakening of convection and the THC, isolate the surface waters from the deeper waters. This leads to much longer response time scales in the Atlantic Ocean near 50°N above 2 km as compared to the Pacific (Figs. 4a,b).

In the cooling case, the THC initially spins up as the climate cools. It remains above the control integration value for about the first 600 yr of the $\frac{1}{2} \times CO_2$ integration. On longer time scales, the equilibrium THC is much weaker than in the control integration [see Stouffer and Manabe (2003) Fig. 7]. This THC response causes a much more complex pattern in the response time scales for this case. Comparing the Atlantic to Pacific response time scales for the $\frac{1}{2} \times CO_2$ case (Figs. 4c,d), the response time scales below about 1.5 km in middle and low latitudes are generally similar in value. These values in the cooling case are generally much smaller than in the warming case (cf. Figs. 4a,c and 4b,d). In the $\frac{1}{2} \times CO_2$ integration above 1.5 km in the low latitudes and above 3 km in high northern latitudes, the Atlantic response time scales are much longer than found at similar locations in the Pacific (Figs. 4c,d). The long response time scales found in the waters in the upper 3 km of the high latitude Atlantic basin in the $\frac{1}{2} \times CO_2$ integration are related to the long response time scale of the THC. The THC response is also associated with changes in oceanic convection and other vertical mixing processes in the ocean (Manabe et al. 1991). These processes are not linearly responding to the changes in radiative forcing, producing the patterns of response and response time scales seen in the Atlantic basin (Fig. 4).

The relatively long response time scales seen in the high latitudes of the North Atlantic Ocean near-surface waters demonstrates the potential for the changes in the THC to moderate the surface climate changes locally. The moderation of the surface climate in the North Atlantic Ocean can last more than 1 century. However, these are only transient effects, as they tend to disappear as the climate system comes into equilibrium with any changes in radiative forcing.

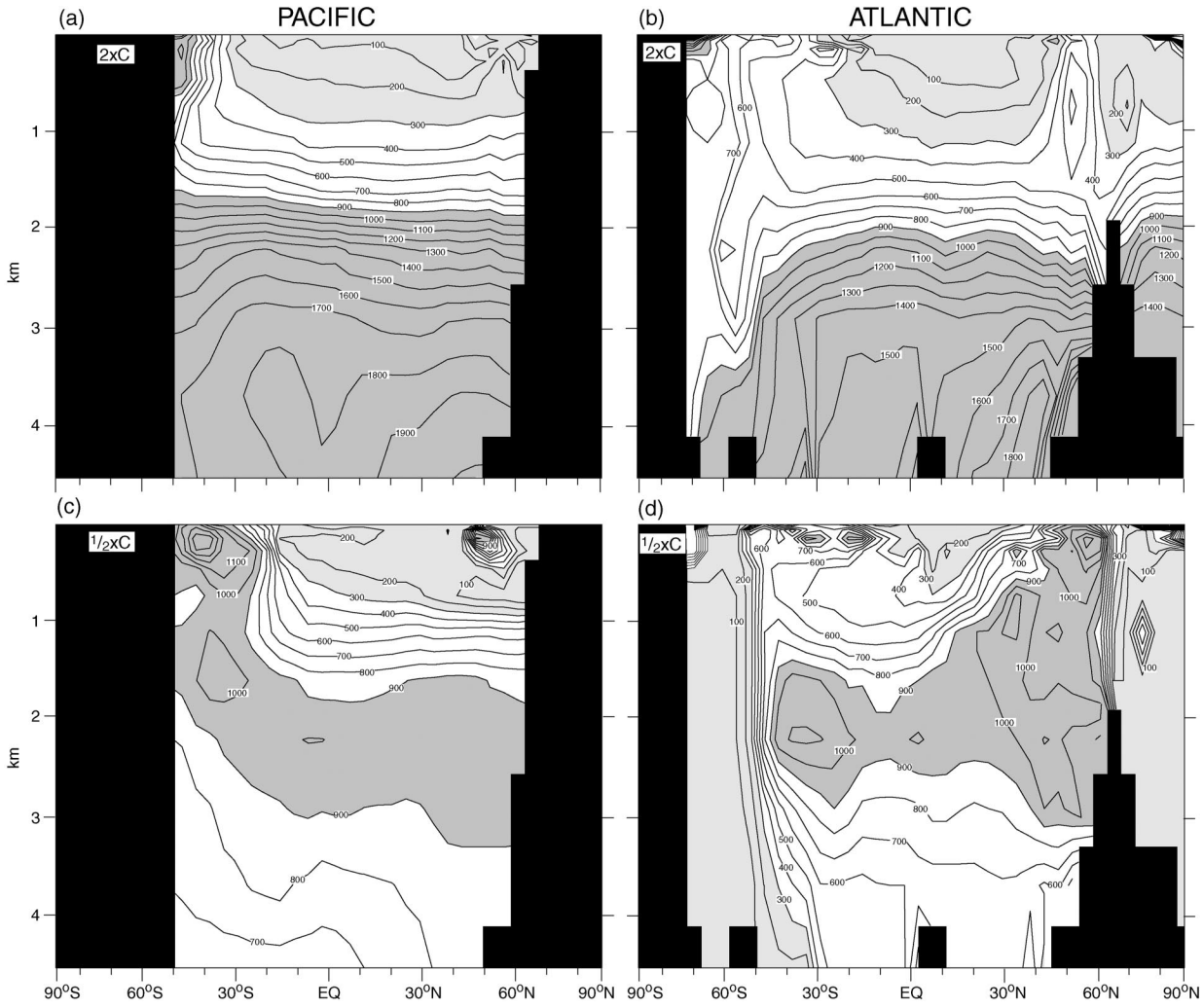

FIG. 4. As in Fig. 3 except for the Pacific (left column) and Atlantic (right column) Ocean basins. (top) Values are obtained from the $2 \times CO_2$ integration, (bottom) $\frac{1}{2} \times CO_2$ integration.

As noted in the introduction, the atmosphere rapidly comes into equilibrium with changes to its lower boundary conditions on time scales of days to weeks. The implication of this statement is that the response time scale of the atmosphere is controlled by the response time scale of the ocean surface mixed layer.

In the Southern Hemisphere, the atmospheric response time scale is much longer than that found in the Northern Hemisphere (Fig. 5). Here, the cooling case generally has a faster response than the warming case. However, the difference in time to reach a given fraction of the total response is relatively small, only about 100 yr. Careful inspection of Figs. 2 and 3 confirms this observation. In the near-surface region of the Southern Hemisphere, the response time scales associated with cooling are generally smaller than those found in the warming case at a given location. The small difference in the response times between the warming and cooling case varies over the course of the integrations.

In the Northern Hemisphere, the situation is different from the Southern Hemisphere described above (Fig. 5). Here the atmospheric response time scales are smaller for the warming case, as compared to the cooling case. One to two thousand years into the integrations, there is a large difference in the time needed to reach a given fraction of the total response. The differences in the time to reach a given fraction of the response may be greater than 500 yr during some periods.

Again, careful inspection of Figs. 2 and 3 confirms this result. The oceanic response times are generally smaller in the Northern Hemisphere near-surface region in the warming case than in the cooling case. As the ocean is being heated (cooled), the stability is increasing (decreasing). As noted above in the warming case, more of the heat is trapped near the surface, leading to larger fractions of the total response. In the cooling case, the heat is mixed through deeper and deeper layers of the ocean, leading to smaller fractions of the total response

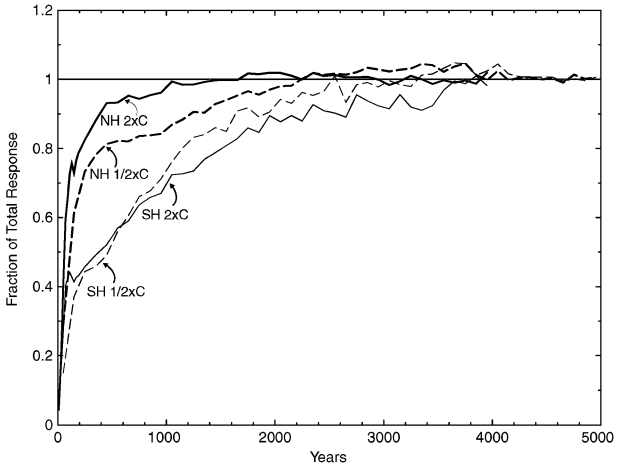

FIG. 5. Time series of the fraction of the total equilibrium, hemispheric mean surface air temperature response (thick lines: Northern Hemisphere values, thin lines: Southern Hemisphere). The solid lines are values from the $2 \times CO_2$ integration and the dashed lines are from the $\frac{1}{2} \times CO_2$ integration.

near the ocean surface. This explanation mainly holds for the Pacific Ocean. Since the Pacific Ocean is much larger than the Atlantic at most latitudes, it dominates the Northern Hemisphere response. As discussed above, the response in the Atlantic is more complex.

Finally, it should be noted that the interhemispheric asymmetry in the atmospheric surface air temperature response time scales first discussed in Manabe et al. (1991) are seen in Fig. 5. They describe results obtained from 100-yr integrations. Here it is seen that the Northern Hemisphere atmospheric response leads the Southern Hemisphere response for much of the integration, until the model reaches a near-equilibrium state. By 600 model years into the integrations, the Northern Hemisphere response is much closer to equilibrium than the Southern Hemisphere. The Southern Hemisphere surface air temperature (SAT) response is about 60% of the total response in both integrations; while the Northern Hemisphere SAT response is more than 80% of the total in both integrations.

5. Discussion

By using temperature response time scales as a surrogate for the climate response time scales, it is shown that the response time scales vary widely with latitude and depth and have a dependence on the sign of the change in radiative forcing. Most of the ocean below 500 m achieves 30% or 70% of the total response almost twice as fast when the changes in forcing are cooling compared to warming the climate system. In the cooling case, the time to achieve 70% of the equilibrium response in the midoceanic regions is about 500 to 1000 yr. In the warming case, this time is 1300–1700 yr. In the high latitudes of the North Atlantic basin, the near-surface response time scales are influenced by changes in the ocean circulation (THC) and other high latitude oceanic mixing processes.

These long response time scales have direct application to the response time scale of sea level. The steric sea level response is the integral of the temperature response throughout the depth of the ocean. The long response time scales noted above, lead to long response time scales for the sea level.

In the Southern Hemisphere, the surface response time is slightly faster in the cooling case. In the Northern Hemisphere, the surface response times are faster in the warming case by more than 500 yr at times during the integrations. Furthermore, the Northern Hemisphere surface response time scales are much faster than either the warming or cooling Southern Hemisphere surface response time scales.

The differing response time scales found in the coupled system can make interpreting various types of paleodata more difficult. Data obtained from different sources (from different ocean basins representing different oceanic depths or atmospheric data) need to be compared very carefully. The response time scales of the physical climate system to a common forcing or signal vary among all these sources.

It is important to note here that the time scales discussed in this study apply only to those of the physical climate system, that is, those obtained from interactions of the ocean–atmosphere–land surface system. Changes in land ice, vegetation, etc. are not considered here. Their inclusion may significantly alter the response time scales presented here. Furthermore, it is noted that orbital changes typically cause radiative forcing changes on time scales longer than the climate response time scales shown here.

The results shown here also have implications for using AOGCMs to model past climates such as the Last Glacial Maximum (LGM). Based on the values obtained from the cooling integration (Fig. 3b), it takes almost 1000 years to reach 70% of the total response in the colder climate throughout most of the World Ocean. Near the surface, it takes a few centuries to reach that fraction of the response (Fig. 5). Running state-of-the-art AOGCMs for hundreds of model years is a very computer-intensive undertaking. New methods need to be found to accelerate the response of the AOGCMs toward equilibrium. It also points to the utility of using less complex coupled models as in Weaver et al. (1998) and Ganopolski et al. (1998) to study these problems. However it needs to be noted that these models suffer many of the same problems as found in this AOGCM and more (coarse resolution, relatively large mixing coefficients, etc.).

The long response time scales in the deep ocean also have implications for initializing AOGCMs to predict future changes in climate due to human activities. Today's ocean state is a mixture of the changes in radiative forcing that have occurred over the past few thousand years. Weaver et al. (2000) have shown that these past

radiative forcing changes can affect future projections of climate through the initial conditions used to make those projections. Much investigation remains in finding the best techniques to initialize AOGCMs for use in making predictions of future climate changes.

It should be noted that the exact length of time for the response of the climate system is dependent on the amount of mixing found in the oceanic component of the AOGCM. The subgrid-scale, oceanic tracer mixing scheme used here is the so-called Cox isopycnal scheme (Redi 1982; Tziperman and Bryan 1993). In the model ocean diapyncal mixing occurs both through the use of diffusion on the grid: horizontal, background diffusion, and vertical diffusion. In addition, the mixing coefficients used in the oceanic component of the AOGCM are relatively large because of the coarse model resolution, much larger than the estimates of the observed values.

Using more realistic mixing schemes and smaller mixing coefficients may lengthen the response time estimates presented here if they lead to less overall mixing. However, the dependence of the response time scales in the mid to deep ocean on the sign of the change in the radiative forcing seems more robust. In the cooling case, some of the increased mixing is resolved by the grid while the response time scale in the warming case seems more related to the magnitude of the diapycnal mixing.

In an attempt to evaluate the oceanic mixing in the model, passive oceanic tracers are used. On the decadal time scale using CFCs, it has been shown by Dixon et al. (1996) that the model CFC simulation is similar to the observations. In section 3, using radiocarbon as an oceanic tracer, it is shown that the model's oceanic mixing on centennial to millennial time scales may be also realistic. However, it is noted that the good present-day tracer simulation may result from compensating model errors.

The good present-day tracer simulation suggests that the quantitative estimates of the response time scales shown here may also be realistic (with the caveat noted above). However, to completely resolve these issues, these integrations will have to be repeated when models using improved mixing schemes and higher resolution become available and can be integrated thousands of model years.

Acknowledgments. This work was inspired through conversations with Anthony Broccoli. Syukuro Manabe, Anthony Rosati, Thomas Delworth, Stephen Griffies, J. Robert Toggweiler, and Jonathan Gregory reviewed earlier versions of the manuscript. J. Robert Toggweiler also provided many of the insights in the radiocarbon section. Laura Stouffer helped edit versions of the manuscript.

REFERENCES

Cubasch, U., and Coauthors, 2001: Projections of future climate change. *Climate Change 2001: The Scientific Basis. Contribution of Working Group I to the Third Assessment Report of the Intergovernmental Panel on Climate Change,* J. T. Houghton et al., Eds., Cambridge University Press, 526–582.

Dixon, K. W., J. L. Bullister, R. H. Gammon, and R. J. Stouffer, 1996: Examining a coupled climate model using CFC-11 as an ocean tracer. *Geophys. Res. Lett.,* **23,** 1957–1960.

——, T. L. Delworth, M. J. Spelman, and R. J. Stouffer, 1999: The influence of transient surface fluxes on North Atlantic overturning in a coupled GCM climate change experiment. *Geophys. Res. Lett.,* **26,** 2749–2752.

England, M. H., 1995: Using chlorofluorocarbons to assess ocean climate models. *Geophys. Res. Lett.,* **22,** 3051–3054.

——, and S. Rahmstorf, 1999: Sensitivity of ventilation rates and radiocarbon uptake to subsurface mixing parameterization in ocean models. *J. Phys. Oceanogr.,* **29,** 2802–2827.

Ganopolski, A., S. Rahmstorf, V. Petoukov, and M. Claussen, 1998: Simulation of modern and glacial climate with a coupled model of intermediate complexity. *Nature,* **391,** 351–356.

Gordon, C. T., and W. F. Stern, 1982: A description of the GFDL spectral model. *Mon. Wea. Rev.,* **110,** 625–644.

Manabe, S., 1969: Climate and the ocean circulation. I. The atmospheric circulation and the hydrology of the earth's surface. *Mon. Wea. Rev.,* **97,** 739–774.

——, R. J. Stouffer, M. J. Spelman, and K. Bryan, 1991: Transient responses of a coupled ocean–atmosphere model to gradual changes of atmospheric CO_2. Part I. Annual mean response. *J. Climate,* **4,** 785–817.

Ostlund, H. G., H. Graig, W. S. Broecker, and D. Spencer, 1987: *Shore Based Data and Graphics.* Vol. 7, *GEOSECS Atlantic, Pacific and Indian Ocean Expeditions,* National Science Foundation, 230 pp.

Redi, M. H., 1982: Oceanic isopycnal mixing by coordinate rotation. *J. Phys. Oceanogr.,* **12,** 1154–1158.

Robitaille, D. Y., and A. J. Weaver, 1995: Validation of sub-grid-scale mixing schemes using CFCs in a global ocean model. *Geophys. Res. Lett.,* **22,** 2817–2920.

Spelman, M. J., and S. Manabe, 1984: Influence of oceanic heat transport upon the sensitivity of a model climate. *J. Geophys. Res.,* **89,** 571–586.

Stouffer, R. J., and S. Manabe, 1999: Response of a coupled ocean–atmosphere model to increasing atmospheric carbon dioxide: Sensitivity to the rate of increase. *J. Climate,* **12,** 2224–2237.

——, and ——, 2003: Equilibrium response of thermohaline circulation to large changes in atmospheric CO_2 concentration. *Climate Dyn.,* **20,** 759–773.

Toggweiler, J. R., and B. Samuels, 1993: New radiocarbon constraints on the upwelling of abyssal water to the ocean's surface. *Global Carbon Cycle,* Springer-Verlag, 333–366.

——, K. Dixon, and K. Bryan, 1989: Simulations of radiocarbon in a course-resolution world ocean model, Part 1: Steady state prebomb distributions. *J. Geophys. Res.,* **94,** 8217–8242.

Tziperman, E., and K. Bryan, 1993: Estimating global air–sea fluxes from surface properties and from climatological flux data using an ocean general circulation model. *J. Geophys. Res.,* **98,** 22 629–22 644.

Weaver, A. J., A. F. Fanning, M. Ebby, and E. C. Wiebe, 1998: The climate of the last glacial maximum in a coupled ocean GCM/energy-moisture balance atmosphere model. *Nature,* **394,** 847–853.

——, P. B. Duffy, M. Ebby, and E. C. Wiebe, 2000: Evaluation of ocean and climate models using present-day observations and forcing. *Atmos.–Ocean,* **38,** 271–301.